UMYU Scientifica, Vol. 4 NO. 3, September 2025, Pp 091 – 096
https://doi.org/10.56919/2543.009
ISSN: 2955 – 1145 (print); 2955 – 1153 (online)
*A periodical of the Faculty of Natural and Applied Sciences, UMYU, Katsina*

ORIGINAL RESEARCH ARTICLE

# Theoretical insight into the prospect of stone–wales defective monolayer silicon carbide for anodes of Na-ion batteries

Nura Ibrahim[1]*, Lawal Mohammed[1], Sadiq Umar[1], Anas Muhammad Salis[1], Abdulrahman Mahruf[1], Fawaz Olamide Ajibola[1]

[1]Department of Physics, Ahmadu Bello University, 810211 Zaria, Nigeria

**ARTICLE HISTORY**

Received May 11, 2025
Accepted September 05, 2025
Published September 30, 2025

**KEYWORDS**

Monolayer, Silicon Carbide, DFT, Na, Anode, Batteries



**ABSTRACT**

In this study, density functional theory (DFT) is employed to investigate how the introduction of Stone–Wales (SW) topological defects can modify the structural, electronic, and electrochemical properties of monolayer silicon carbide (SiC) for sodium (Na) ion storage. Results show that SW-defective SiC (SiC-SW) is both energetically feasible and dynamically stable, with enhanced electronic conductivity compared to pristine SiC. Na adsorption energy improves from 0.85 eV (pristine) to – 0.89 eV (SiC-SW), while the diffusion barrier remains low (0.88 eV). SiC-SW achieves a maximum Na storage capacity of 300 mAh $g^{-1}$ with an average open circuit voltage (OCV) of 0.44 V. These findings suggest that SW defect engineering could make SiC a competitive anode material for next-generation Na-ion batteries.

## INTRODUCTION

Lithium-ion batteries (LIBs) dominate the energy storage market because of their high energy density and long cycle life (Finkelstein *et al.*, 2024). However, concerns over lithium's limited supply, uneven geographical distribution, and rising cost have driven researchers to explore alternative chemistries such as sodium-ion, potassium-ion, and magnesium-ion batteries (Bella *et al.*, 2021; Lee *et al.*, 2025; Riza *et al.*, 2024). Sodium-ion batteries (SIBs) are particularly attractive due to sodium's abundance and similar electrochemical behaviour to lithium (Qiu *et al.*, 2025).

The primary bottleneck in SIB development lies in the anode. Graphite, the standard LIB anode, poorly accommodates $Na^+$ due to its larger ionic radius and sluggish diffusion, resulting in a low capacity. Yet, there are currently very few good candidate materials for the anode of SIBs (Abraham, 2020; Liang *et al.*, 2024). Therefore, it is imperative to find better anode materials for SIBs with increased capacity by using a similar approach to investigating the anode materials of LIBs. To this effect, two-dimensional (2D) materials have drawn attention due to their large surface area, enhanced ion accessibility, and tunable electronic characteristics (Martins *et al.*, 2025; Wang *et al.*, 2023).

Monolayer silicon carbide (SiC) stands out in this category due to its chemical stability, mechanical strength, and intrinsic bandgap. Moreover, defect engineering, especially the introduction of Stone-Wale defects (SWDs), can significantly alter its surface chemistry and electronic structure. Such defects, generated by a 90° rotation of a Si–C bond, create pentagon–heptagon pairs in the lattice, modifying charge distribution and potentially enhancing ion adsorption and transport (Fan *et al.*, 2024; Kamyabmehr *et al.*, 2021). For example, Thomas *et al.* (2020) explored the potential of boron carbide ($BC_3$) monolayer with point and topological defects as an anode material in alkali metal-based lithium (Li) ion batteries using first-principles calculations. Their results showed that, compared to its pristine form, $BC_3$ with SW-type topological defects had better Li binding energy and stronger structural stability.

Additionally, unlike traditional graphite anodes, defect-filled $BC_3$ monolayers exhibited a high theoretical specific capacity of 1287 mAh $g^{-1}$, low diffusion energy barriers, and increased electrical conductivity. Recently, Al-sanjari *et al.* (2022) also examined how SWD affects the structure, Mg adsorption, diffusion, and electrochemical properties of boron nitride nanosheets (BNNs). Their findings indicate that, compared to pure BNNs, SW-BNNs have higher electrical conductance, Mg-adsorption ability, and mobility. In addition, the maximum theoretical capacity of SW-BNNs was roughly four times greater than that of pristine BNNs. These findings highlight the significance of SWD in enhancing electronic conductivity, metal

**Correspondence:** Nura Ibrahim. Department of Physics, Ahmadu Bello University, 810211 Zaria, Kaduna Satae, Nigeria. ✉ inura5080@gmail.com.

**How to cite**: Ibrahim, N., Mohammed, L., Umar, S., Muhammad, A. S., Mahruf, A. & Olamide, F. A. (2025). Theoretical insight into the prospect of stone–wales defective monolayer silicon carbide for anodes of Na-ion batteries. *UMYU Scientifica*, 4(3), 91 – 96. https://doi.org/10.56919/2543.009

adsorption, and diffusion, as well as the overall storage capacity of monolayers.

This work employs first-principles DFT simulations to investigate the feasibility of using SiC-SW as a Na-ion battery anode. The analysis includes structural stability, electronic properties, Na adsorption energies, ion diffusion pathways, capacity, and voltage profiles.

## SIMULATION DETAILS

All calculations were performed using the Quantum ESPRESSO package (Giannozzi *et al.*, 2009). Electron-ion interactions were modelled with the projected augmented wave (PAW) pseudopotentials, and the exchange and correlation effects were described with the generalized gradient approximation (GGA) using the Perdew Burke Ernzerhof (PBE) functional (Perdew *et al.*, 1996). Van der Waals interactions were included via Grimme's D3 dispersion correction (Grimme *et al.*, 2016) to better account for the weak Na-substrate interactions.

Convergence tests established a kinetic energy cutoff of 40 Ry and k-point meshes of 4×4×1 for geometry optimization and 13×13×1 for electronic density of states calculations. Structural relaxation proceeded until residual forces were below $10^{-3}$ eV/Å and total energy changes were under $10^{-6}$ eV. Adsorption energies ($E_{Ad}$) were computed relative to the pristine substrate and isolated Na atoms using Eqn. 1, by adopting a 3x3 supercell of the SiC containing 18 atoms. To avoid interaction between periodic images, a minimum vacuum space of 15Å is set along the vertical direction.

$$E_{Ad} = \frac{\left(E_{(SiC-SW+Na_n)} - E_{(SiC-SW)} - nE_{(Na)}\right)}{n} \quad (1)$$

where; $E_{(SiC-SW+Na_n)}$, $E_{SiC-SW}$, $E_{(Na)}$ and n are the total energy of SiC-SW with n-adsorbed Na atom(s), the total energy of SiC-SW, the total energy of a single Na atom, and the total number of Na atoms adsorbed. The total energy of a single Na was obtained from an optimized unit cell of its cubic bulk structure. A negative value of $E_{Ad}$ implies an energetically feasible adsorption of Na on the surface of the SiC-SW. Maximum Na adsorption on the surface of the SiC-SW substrate is determined from the differential adsorption energy ($E_{diff}$):

$$E_{diff} = E_{Na_xSiC-SW} - E_{Na_{(x-1)}SiC-SW} - E_{Na} \quad (2)$$

where $E_{Na_xSiC-SW}$, is the energy of $x$ number of Na ions adsorbed on SiC-SW, $E_{Na_{(x-1)}SiC-SW}$, is the energy of ($x$ − 1) number of Na ions adsorbed on SiC-SW and $E_{Na}$, is the energy of a single Na.

Diffusion barriers and minimum energy paths were obtained via the climbing-image nudged elastic band (CI-NEB) method (Henkelman & Jónsson, 2000). The open circuit voltage (OCV) was determined from the total energy differences (Eqn. 3) (Ibrahim *et al.*, 2024) and theoretical capacity, calculated using Faraday's law (Eqn. 4).

$$OCV = -\frac{\left(E_{(SiC-SW+Na_n)} - E_{(SiC-SW)} - nE_{(Na)}\right)}{ne} \quad (3)$$

where e is the charge of an electron.

$$Capacity = \frac{xF}{nM_{SiC-SW}} \quad (4)$$

where F is Faraday's constant and x is the number of electrons participating in the electrochemical reaction. The SiC-SW's molar mass and concentration are denoted by M and n, respectively.

## RESULTS AND DISCUSSION

### Structural and Electronic Properties

The calculations proceeded with a full relaxation of the atomic structure of the pristine SiC. The relaxed SiC substrate forms a planar honeycomb lattice with Si–C bonds of 1.79 Å and bond angles of 120° (Fig. 1A). The calculated lattice parameters $a = b = 3.09$ Å are consistent with the previously reported experimental and theoretical values of 3.08 Å (Lin *et al.*, 2015) and 3.90 Å (Ibrahim *et al.*, 2022; Ibrahim *et al.*, 2024). The SWD is then introduced by rotating a Si–C bond of the optimized supercell of the pure SiC. A complete structural optimization of this structure is performed again, as shown in Fig. 1D. To assess the possibility of an experimental realization, the formation energy is calculated from the total energy difference between the defective and pure SiC substrate (Tian *et al.*, 2020). The calculated formation energy of 5.51 eV falls within accessible range for other 2D materials, such as hexagonal boron nitride (4.08 - 6.08 eV) (Hamdi *et al.*, 2020; Thomas *et al.*, 2015) and Silicene (2.57 eV). This suggests that the SiC-SW is likely to be experimentally feasible.

Fig. 1 (B &C) shows the electronic band structure and partial density of states (PDOS) of pristine SiC, which is an indirect bandgap semiconductor. Its computed energy gap of 2.53 eV is in agreement with the 2.72 eV previously reported by He *et al.* (2021). The valence band is dominated by C 2p states and the conduction band by Si 2p states. Consistently, SiC-SW is semiconducting but with a much shallower bandgap of 0.78 eV, between the conduction and valence bands (Fig. 1E). Additionally, the PDOS (Fig. 1F) further shows that the major contribution of the C and Si 2p states in the respective valence and conduction bands is maintained. A similar change in the energy gap upon defect formation has been previously reported by Kamyabmehr *et al.* (2021).

### Na Adsorption and Diffusion Properties

The adsorption of Na on the surface of SiC-SW is then assessed by first identifying the preferable adsorption site for a single Na atom. Various possible adsorption sites are available on the SiC-SW, as shown in Fig. 2A. Inserting test Na atoms on these sites and optimizing the structure, we identified the preferred adsorption site to be at the top of the heptagonal ring (Fig. 2B), with a calculated $E_{Ad}$ of -0.89 eV. This moderately high energy suggests a good adsorption of Na on the SiC-SW substrate. In addition to the preferred adsorption sites, a

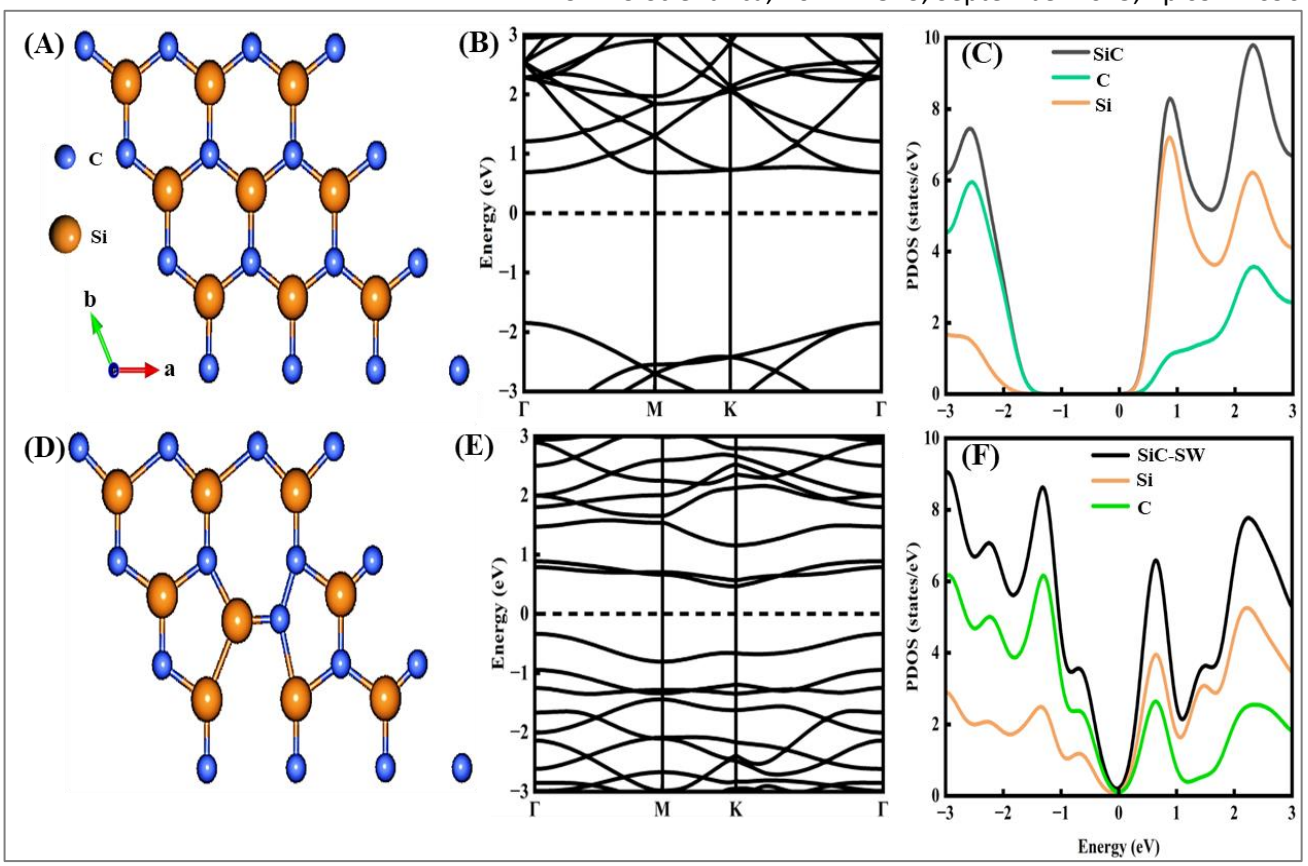


**Fig. 1: (A&D), optimized structures of 3x3x1 supercell of SiC and SiC-SW. (B&C) and (E&F), Band structure and partial density of states of SiC and SiC-SW.**

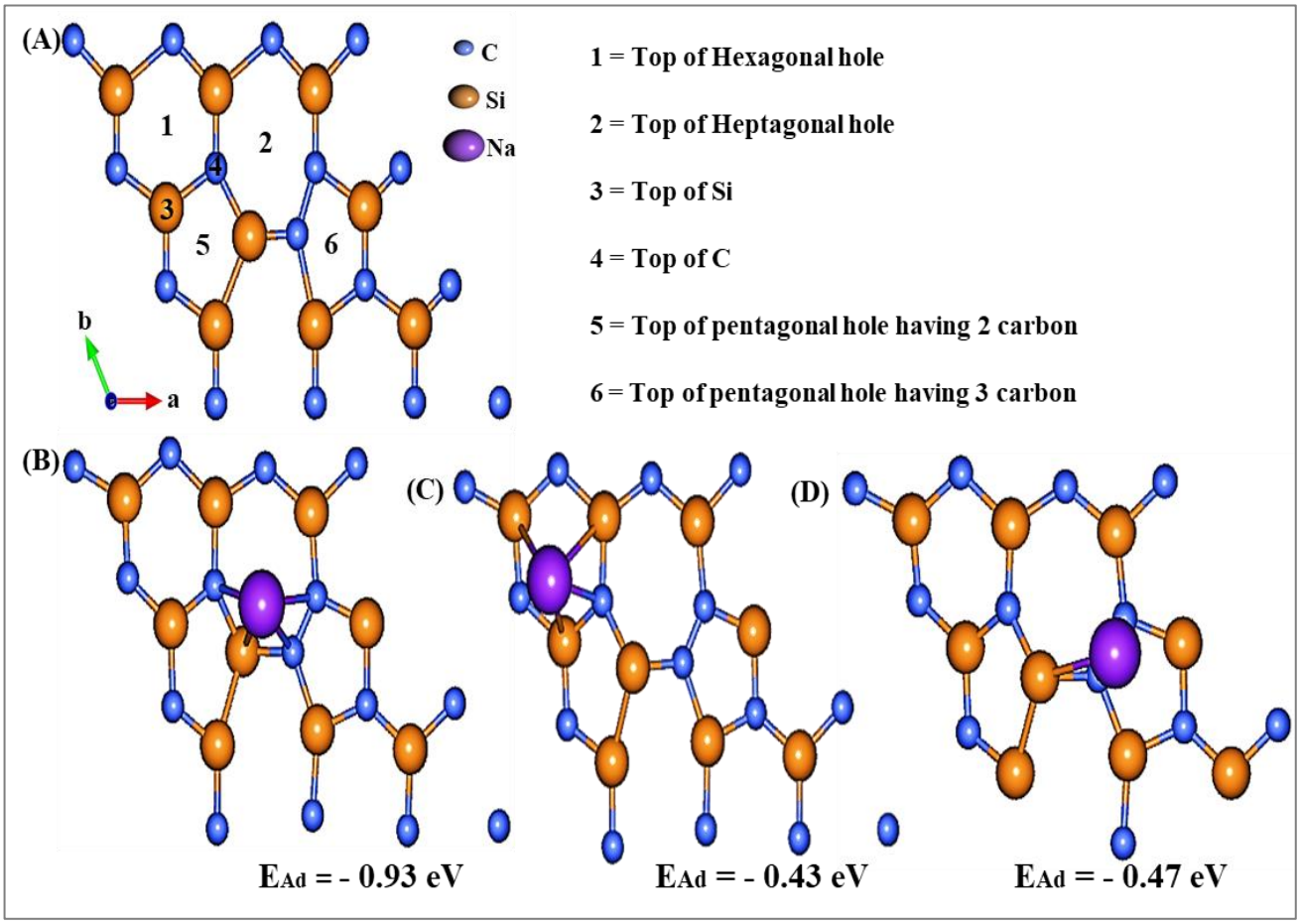


**Fig. 2: (A) Possible adsorption points on the surface of SiC-SW. (B) Optimized most preferred adsorption point for single Na adsorption on SiC-SW. (C&D) Optimized metastable adsorption sites for single Na adsorption on SiC-SW.**

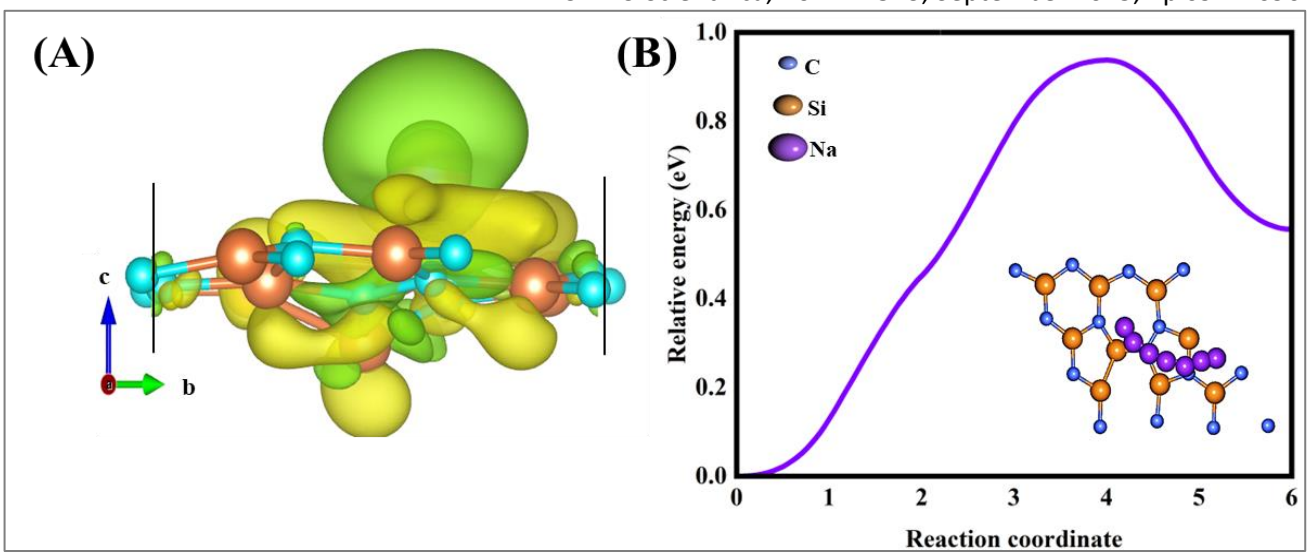


**Fig. 3: (A) Differential charge density plot of Na-adsorbed SiC-SW. (B) Diffusion energy barrier and pathway for Na ion.**

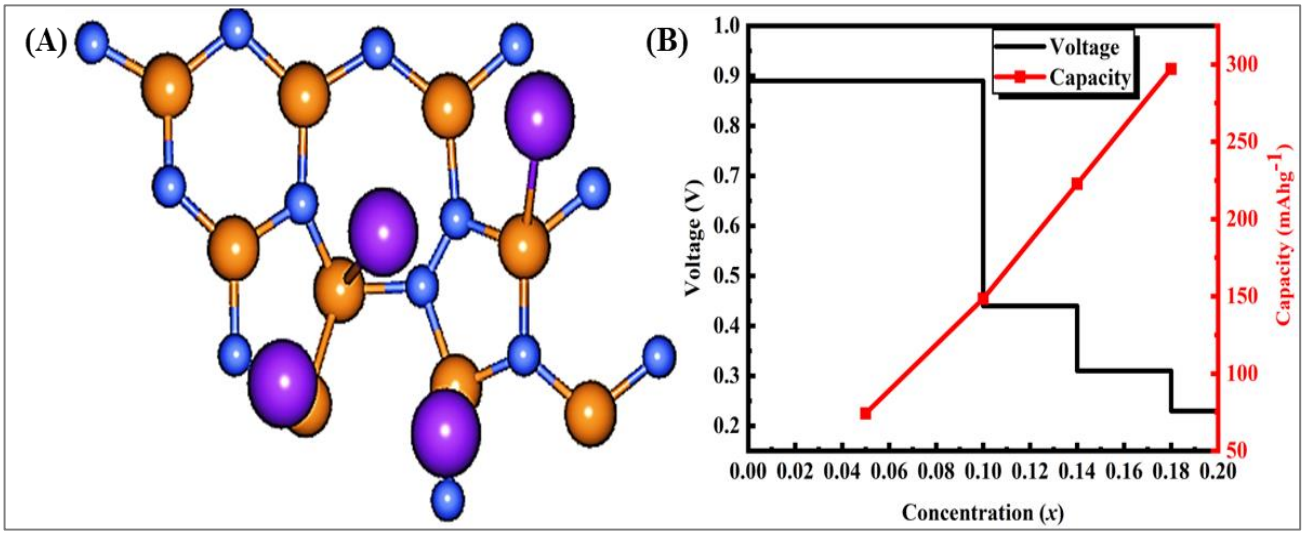


**Fig. 4: (A) Optimized structure of four Na atoms (maximum) adsorbed on SiC-SW. (B) OCV and capacity against Na concentration.**

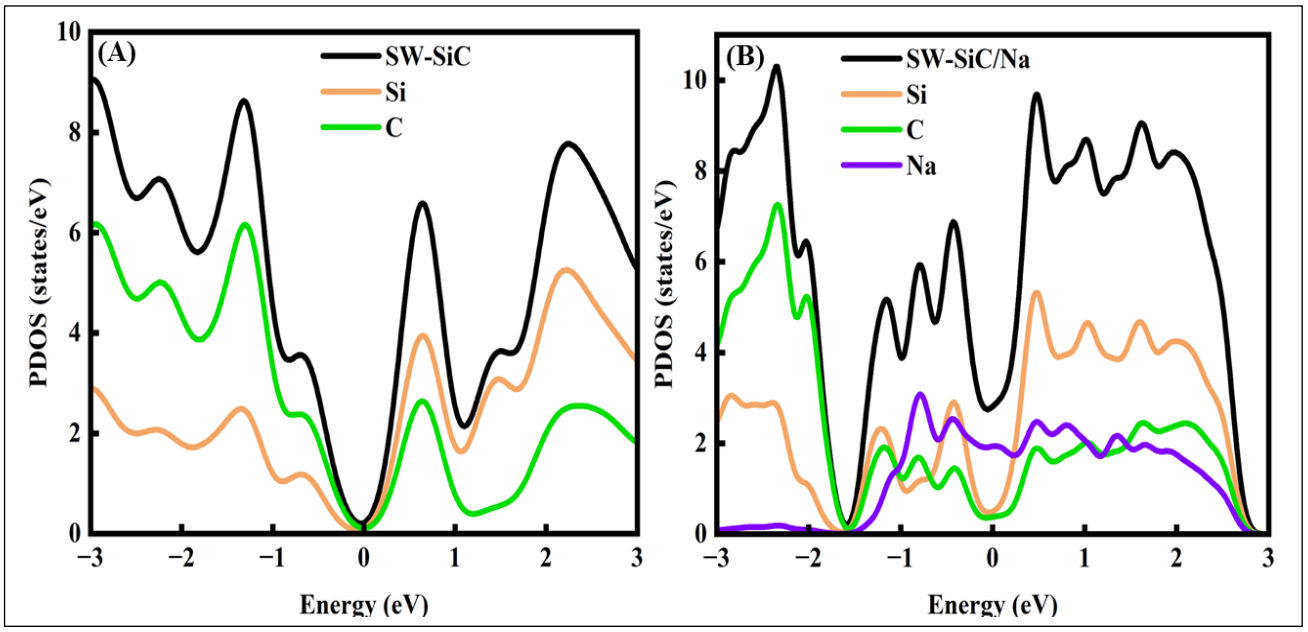


**Fig. 5: (A&B) PDOS of pristine SiC-SW and SiC-SW/Na**

few other metastable adsorption points were identified (Fig. 2C&D). To better understand the nature of the interaction between Na and the substrate, differential charge density was calculated using Eqn. 5, and the associated plot is shown in Fig. 3A.

$$\Delta\rho = \rho_{Na+SiC-SW} - (\rho_{SiC-SW} + \rho_{Na}) \quad 5$$

where $\rho_{Na+SiC-SW}$ , $\rho_{SiC-SW}$ and $\rho_{Na}$ are the charge densities of SiC-SW plus Na, SiC-SW, and Na, respectively. From the plot, it is observed that charges tend to cluster on the surface of SiC-SW and deplete on the Na atom, showing electron drift from the Na to the SiC-SW substrate.

Furthermore, the ease of migration of Na on the SiC-SW surface is assessed by calculating the diffusion energy barrier and minimum energy pathway. Easy migration, as well as good charging and discharging rates on the surface of the substrate, is identified by low energy barriers. The energy barrier for the Na diffusion on the SiC-SW is calculated to be 0.88 eV along the pathway shown in Fig. 3B, aligning with existing literature for other substrates such as biphenylene (0.76 eV) (Xu *et al.*, 2024) and 1T-$MoS_2$ (0.70 eV) (Massaro *et al.*, 2021). Also, the minimal low diffusion energy of the SiC-SW highlights its good rate capability for anode application.

### Storage Capacity, Voltage Profile and Electronic Transition

The theoretical storage capacity of the SiC-SW structure is analyzed by sequentially inserting additional Na atoms at available adsorption sites. For each Na atom added, the atomic positions are fully relaxed, and the tendency of Na atoms to adsorb on the substrate is evaluated using Eqn. 1. As previously mentioned, the preferred adsorption site for a single Na atom is at the top of the heptagon hole. For two Na atoms, the optimized structure includes one Na atom at the top of the heptagon site and another on top of Si, with a calculated energy of – 0.44 eV. Generally, we observed a decrease in adsorption energy as Na concentration increases on the substrate surface. This can be attributed to increased repulsion between Na atoms. At a concentration of four Na atoms, which corresponds to a single layer of Na on the SiC-SW (Fig. 4A), the $E_{Ad}$ is – 0.02 eV. Adding another Na atom results in an $E_{diff}$ of 0.07 eV, indicating an endothermic reaction. Therefore, four Na atoms are considered the maximum adsorption limit for SiC-SW, corresponding to a storage capacity of 300 mAh/g. The capacity of SiC-SW is comparable with that of SnS (375 mAh/g) and exceeds that of $VS_2$ (232.91 mAh/g) (Putungan *et al.*, 2016).

Accordingly, Fig. 4B illustrates the OCV curve of SiC-SW in Na-ion batteries, with x representing the number of Na ions adsorbed per total number of atoms. As shown, the OCV decreases with increasing Na concentration, due to heightened ionic repulsion and Na/SiC-SW attraction. The initial voltage is 0.23 V, gradually decreasing to 0.89 V at higher concentrations. Overall, an average voltage of 0.44 V is maintained within the SiC-SW, which, compared to other previous substrates like $Si_3C$ (0.55 V) (Hu *et al.,* 2022) and BSi (0.53 V) (Wang et *al.,* 2023), is lower. This highlights the potential of SiC-SW as a good substrate for anode in Na-ion batteries, as it can achieve a higher output voltage.

It should be noted that these results are obtained from DFT calculations at 0 K and do not account for temperature, entropy, or electrolyte effects, which may influence electrochemical performance under practical conditions.

Lastly, the effect of inserting Na ions on the electronic structure is investigated. The PDOS of both pure SiC-SW and SiC-SW with Na adsorbed is displayed in Fig. 5(A&B). It can be observed that the adsorption of Na on the surface of SiC-SW causes a transition from semiconductor to metal, indicating increased electrical conductivity on the substrate with Na ion insertion, which is in line with previous reports from literature (Peng *et al.*, 2024).

## CONCLUSION

DFT approach was employed to investigate the potential of SiC-SW as an anode material for SIBs. The SiC-SW structure exhibits a formation energy of 5.51 eV and an indirect shallow band gap of 0.78 eV. Sodium atoms adsorb onto the surface with a moderately strong adsorption energy of –0.89 eV, while Na migration occurs readily with a low diffusion barrier of 0.88 eV. The SiC-SW layer demonstrates a theoretical storage capacity of up to 300 mAh $g^{-1}$ and an average OCV of 0.44 V. The combination of favorable Na adsorption, low diffusion barrier, suitable OCV, and moderate storage capacity underscores the promise of SiC-SW as a potential anode material for SIBs.

## FUNDING

This work was funded by the TETFUND Institution-based research (TETF/DR&D/UNI/ZARIA/IBR/2024/BATCH 8/15).

## REFERENCES

Abraham, K. M. (2020). How Comparable Are Sodium-Ion Batteries to Lithium-Ion Counterparts? *ACS Energy Letters*, *5*(11), 3544-3547. [Crossref]

Adnan Al-Sanjari, H., Reaad, S., Sabri Abbas, Z., Rayid, R., Abdullaha, S. A. H., Hachim, S. K., Kadhim, M. M., Mahdi Rheima, A., & Ismael Ibrahim, A. (2022). Exploring the role of Stone-Wales defect in boron nitride nano-sheet as a anode Mg-ion batteries. *Inorganic Chemistry Communications*, *146*, 110098. [Crossref]

Bella, F., De Luca, S., Fagiolari, L., Versaci, D., Amici, J., Francia, C., & Bodoardo, S. (2021). An Overview on Anodes for Magnesium Batteries: Challenges towards a Promising Storage Solution for Renewables. *Nanomaterials*, *11*(3).

Fan, L., Wu, Y., Liu, F., Wang, Y., Wu, Y., Wei, X., & Li, L. (2024). Effects of defects on the structure, electronic and elastic properties of Nb2GaC: A first principle calculations. *Vacuum*, *230*, 113695. [Crossref]

Finkelstein, S. H., Ricci, M., Bötticher, T., & Schmidt-Rohr, K. (2024). How lithium-ion batteries work conceptually: thermodynamics of Li bonding in idealized electrodes [10.1039/D4CP00818A]. *Physical Chemistry Chemical Physics*, *26*(36), 24157-24171. [Crossref]

Giannozzi, P., Baroni, S., Bonini, N., Calandra, M., Car, R., Cavazzoni, C., Ceresoli, D., Chiarotti, G. L., Cococcioni, M., & Dabo, I. (2009). QUANTUM ESPRESSO: a modular and open-source software project for quantum simulations of materials. *Journal of physics: condensed matter*, *21*(39), 395502.

Grimme, S., Hansen, A., Brandenburg, J. G., & Bannwarth, C. (2016). Dispersion-Corrected Mean-Field Electronic Structure Methods. *Chemical Reviews*, *116*(9), 5105-5154. [Crossref]

Hamdi, H., Thiering, G., Bodrog, Z., Ivády, V., & Gali, A. (2020). Stone–Wales defects in hexagonal boron nitride as ultraviolet emitters. *npj Computational Materials*, *6*(1), 178. [Crossref]

Henkelman, G., & Jónsson, H. (2000). Improved tangent estimate in the nudged elastic band method for finding minimum energy paths and saddle points. *The Journal of Chemical Physics*, *113*(22), 9978-9985. [Crossref]

Ibrahim, N., Mohammed, L., & Ahmed, R. (2022). Graphene-like silicon carbide layer for potential safe anode lithium ion battery: A first principle study. *Science Talks*, *4*, 100075. [Crossref]

Ibrahim, N., Mohammed, L., Umar, S., Ceresoli, D., & Zhang, Q. (2024). 2d van der Waal SiC/borophene heterostructure as a promising anode for high-capacity Li ion battery: First principles study. *FlatChem*, *47*, 100729. [Crossref]

Kamyabmehr, S., Zoriasatain, S., & Farhang Matin, L. (2021). Effects of Stone-Wales defects on optical properties of silicene: DFT study. *Optik*, *241*, 166952. [Crossref]

Lee, J., Lee, J., & Lim, E. (2025). Recent progress and challenges in potassium-ion battery anodes: towards high-performance electrodes. *Science and Technology of Advanced Materials*, *26*(1), 2518746. [Crossref]

Liang, J., Wei, C., Huo, D., & Li, H. (2024). Research progress on modification and application of two-dimensional anode materials for sodium ion batteries. *Journal of Energy Storage*, *85*, 111044. [Crossref]

Lin, S., Zhang, S., Li, X., Xu, W., Pi, X., Liu, X., Wang, F., Wu, H., & Chen, H. (2015). Quasi-Two-Dimensional SiC and SiC2: Interaction of Silicon and Carbon at Atomic Thin Lattice Plane. *The Journal of Physical Chemistry C*, *119*(34), 19772-19779. [Crossref]

Martins, N. F., Laranjeira, J. A., & Sambrano, J. R. (2025). OCD-graphene: a 2D carbon allotrope with high theoretical capacity for sodium-ion batteries. *FlatChem*, *53*, 100910. [Crossref]

Massaro, A., Pecoraro, A., Muñoz-García, A. B., & Pavone, M. (2021). First-Principles Study of Na Intercalation and Diffusion Mechanisms at 2D MoS2/Graphene Interfaces. *The Journal of Physical Chemistry C*, *125*(4), 2276-2286. [Crossref]

Peng, Q., Rehman, J., Ullah, M., Tighezza, A. M., Hanif, M. B., Shibl, M. F., & Dai, J. (2024). Anchoring of K and Na on the surface of a novel SiC monolayer: First-principles predictions. *Journal of Energy Storage*, *104*, 114435. [Crossref]

Perdew, J. P., Burke, K., & Ernzerhof, M. (1996). Generalized gradient approximation made simple. *Physical review letters*, *77*(18), 3865.

Qiu, S., Meng, L., An, L., Wu, Q., Cui, S., Hao, Z., Zhao, Y., & Zhang, H. (2025). Research progress of transition metal oxides as anode materials for sodium ion batteries. *Journal of Energy Storage*, *132*, 117834. [Crossref]

Riza, S. A., Xu, R.-g., Liu, Q., Hassan, M., Yang, Q., Mu, D.-b., Li, L., Wu, F., & Chen, R.-j. (2024). A review of anode materials for sodium ion batteries. *New Carbon Materials*, *39*(5), 743-769. [Crossref]

Thomas, S., Ajith, K. M., Chandra, S., & Valsakumar, M. C. (2015). Temperature dependent structural properties and bending rigidity of pristine and defective hexagonal boron nitride. *Journal of physics: condensed matter*, *27*(31), 315302. [Crossref]

Thomas, S., Madam, A. K., & Zaeem, M. A. (2020). Stone–Wales Defect Induced Performance Improvement of BC3 Monolayer for High Capacity Lithium-Ion Rechargeable Battery Anode Applications. *The Journal of Physical Chemistry C*, *124*(11), 5910-5919. [Crossref]

Tian, B., Du, W., Chen, L., Guo, J., Shu, H., Wang, Y., & Dai, J. (2020). Probing pristine and defective NiB6 monolayer as promising anode materials for Li/Na/K ion batteries. *Applied Surface Science*, *527*, 146580. [Crossref]

Wang, S., Wu, Y., Ye, X., & Sun, S. (2023). Predict low energy structures of BSi monolayer as high-performance Li/Na/K ion battery anode. *Applied Surface Science*, *609*, 155222. [Crossref]

Xu, Y., Fu, Y., Gong, X., Xu, J., & Liu, W. (2024). Insights into Na ion adsorption and diffusion in biphenylene as an anode material for sodium-ion batteries: A first-principles study. *Materials Today Communications*, *41*, 110394. [Crossref]